Available online at www.sciencedirect.com

**ScienceDirect**

journal homepage: www.elsevier.com/locate/he

**ELSEVIER**

# Hydrogen accumulation and diffusion in cylindrical-shaped pipeline steels with coating defects

*Michael Auinger* [a,*], *Markus Büchler* [b,**], *Hanns-Georg Schöneich* [c], *Christian Gierl-Mayer* [a], *Herbert Danninger* [a]

[a] *Institute of Chemical Technologies and Analytics, Technische Universität Wien, Getreidemarkt 9, 1040 Vienna, Austria*
[b] *Schweizerische Gesellschaft für Korrosionsschutz, Technoparkstrasse 1, 8005 Zurich, Switzerland*
[c] *Formerly at: Open Grid Europe GmbH, Kallenbergstrasse 5, 45141 Essen, Germany*

## HIGHLIGHTS

- Cathodic corrosion protection can lead to accumulation of hydrogen in the material.
- Corrosion protection current densities from ISO norms may already lead to H accumulation.
- Analytical model for diffusion in cylidrical geometry developed, including coating defect areas.
- Influence and interplay between parameters such as time, position, diffusion, and kinetic hydrogen uptake quantified.
- Simulations verified against experiments as well as limiting special cases and show good agreement.

## ARTICLE INFO

## ABSTRACT

The effective diffusion of hydrogen in a cylindrical geometry, mimicking a pipe with a coating defect, was investigated by modelling and verified experimentally. Analytical solutions for the extreme cases of no hydrogen uptake and constant hydrogen uptake were developed. Simulations showed less than 5% error, when compared to two well-documented reference cases for diffusion. The intermediate case of modelling kinetic controlled hydrogen uptake was investigated and the effects of time, position, effective diffusion coefficient, corrosion protection current density and their binary interactions, were reported. Modelling results show, that certain parameter combinations such as effective hydrogen diffusion coefficients between $10^{-11}$ - $10^{-9.5}$ m$^2$ s$^{-1}$, particularly in combination with a hydrogen uptake $j_H$ of more than 0.1 A m$^{-2}$, may lead to locally increased hydrogen concentrations in the material.

\* *Corresponding author.*
\*\* *Corresponding author.*
  E-mail addresses: michael.auinger@tuwien.ac.at (M. Auinger), markus.buechler@sgk.ch (M. Büchler).
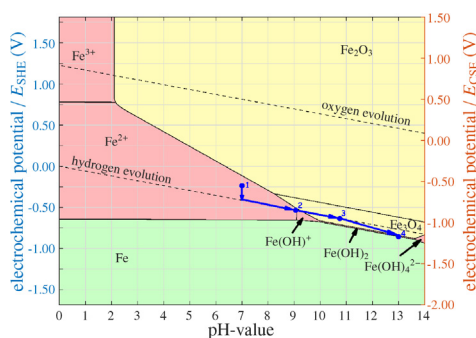
## Introduction

Cathodic protection (CP) is statutory for high pressure gas- and oil-pipelines and is also frequently used for water pipelines and buried containers. The mechanism of cathodic protection as well as the physico-chemical processes associated with the protection criteria are a frequent topic of investigations. In general, the increase of the surface pH as a result of the application of cathodic protection and the control of the electrode potential by the hydrogen electrode are well established [1–3]. Even small cathodic current densities in the range of 10 mA m$^{-2}$ result in the formation of alkaline species at the steel surface, leading to a significant increase of the pH-value [4]. This increase of the pH favours the formation of a protective passive film, which significantly limits any further corrosion [5–8]. Based on thermodynamic and kinetic data, the applicable criteria for cathodic protection can readily be explained [9]. The pH increase and the mass transport are hence the main controlling processes. The relevant aspects associated with cathodic protection are illustrated in Fig. 1.

Starting from the corrosion potential (point 1 in Fig. 1), the application of cathodic protection results in oxygen consumption and polarization to the equilibrium line for hydrogen evolution as indicated with the blue arrow. This activation polarization does not provide corrosion protection as can readily be concluded from the position within the corrosion domain of the Pourbaix diagram that is usually associated with corrosion rates in the range of 0.1 mm per year. In anaerobic conditions, the corrosion potential will be cathodic of the hydrogen evolution line near potentials of $-0.85$ V$_{CSE}$ (i.e. the potential in point 2 but for higher bulk pH-values), as reported by [11]. In well-aerated conditions, the

oxygen reduction reaction instead of the hydrogen evolution becomes rate determining. These conditions are usually observed for pipeline steels in soil. This leads to a shift towards positive potentials and significant polarization cathodic of the hydrogen evolution line is only possible at increased cathodic current densities which will result in an increase of the pH-value, leading to a shift into the passivity domain. In both cases, the accumulation of hydroxide ions over time generates conditions that are conducive to the formation of a passive film as illustrated with the blue arrow in Fig. 1. This passive film formation causes corrosion rates that are usually in the range of 0.01 mm per year [1,12,13]. Since the hydrogen equilibrium potential depends on the pH-value, which in turn can be found by following the hydrogen evolution line in Fig. 1, the pH-value at the steel surface can directly be determined based on the IR-free potential (*immediate off potential reading*, the potential at the steel surface without the drop of resistance by the soil) and is usually reported versus a saturated copper sulphate reference electrode (CSE electrode). This has been discussed in detail by Angst et al. [1]. For this reason, the relevant protection potentials for iron can be explained as follows.

- the potential of $-0.85$ V$_{CSE}$ corresponds to a pH of 9 (point 2 in Fig. 1), which is, according to Fig. 1, sufficient for achieving passivity
- the potential of $-0.95$ V$_{CSE}$ corresponds to a pH of 10.6 (point 3 in Fig. 1), which allows for passivity even in aggressive electrolytes
- however, a potential of $-1.2$ V$_{CSE}$ corresponds to a pH of more than 12.5, which may cause problems with the adhesion of coatings, exposing iron (point 4 in Fig. 1) and leading to excessive hydrogen evolution with current densities in the range of 1 A m$^{-2}$ [14]

It immediately follows, that meeting these potentials for cathodic protection is associated with a certain level of hydrogen evolution. The formation of hydrogen and its association with effective cathodic protection has already been pointed out by Kuhn in 1930 [15]. According to ISO 15589-1 hydrogen embrittlement only needs to be considered on high strength non-alloyed and low-alloyed steels with designed yield strength above 550 N mm$^{-2}$. However, it is well known that near-neutral stress corrosion cracking is associated with hydrogen formation in many commercial steel grades, thus also contributing to the intergranular cracking process [16] for a steel which is considered non-critical by the ISO-definition. This raises the question whether hydrogen generation at coating defects of pipelines may lead to hydrogen loading and the influence of hydrogen transport [17–19] within the pipeline steel as a function of time. Measuring the kinetics of hydrogen uptake is a complex but also highly relevant activity. Due to local pH-shifts near the surface [4], the local ion concentrations may exceed the solubility limit, thus leading to the formation of oxides, hydroxides and other precipitates such as earth alkali carbonates which are partially mixed with hydroxides and chlorides (e.g in seawater). Whilst these precipitates may hamper the kinetics of hydrogen uptake, the purpose of this study is to investigate by means of mathematical modelling and experiments



**Fig. 1 — Pourbaix-diagram for iron [10] at 1µM Fe$^{2+}$ in solution as function of electrochemical potential vs. standard hydrogen electrode (SHE, left) and as function of copper sulphate electrode (CSE, right). Different colours were used to highlight the regions of material protection (green), passivation (yellow) and corrosion (red). The vertical blue arrow shows the effect of activation polarization while the blue arrows along the hydrogen evolution line illustrate the contribution of concentration polarization. The blue dots (2), (3) and (4) indicate the position of the potentials for cathodic protection (CP), given in ISO 15589–1.**

whether cathodic protection may potentially contribute to the hydrogen loading of steels as a function of distance from the coating defect.

## Mathematical modelling

The mathematical model is obtained as an explicit analytic solution for the local hydrogen concentration $c$ as a function of position and time. Compared to numerical solutions from standard FEM-solvers, an analytical solution offers the advantage to study parameter variations more effectively. The following symbols were used throughout this study:

$c$ .... ... ... .... hydrogen concentration in mol m$^{-3}$
$c_0$.... ... ... .... initial hydrogen concentration in mol m$^{-3}$
$c_\infty$.... ... ... ... final hydrogen concentration in mol m$^{-3}$
$\beta_H$.... ... ... ... weight fraction of hydrogen in ppm.wt
$\mathbb{D}$.... ... ... .... diffusion coefficient in m$^2$ s$^{-1}$
$t$.... ... ... ...... time in s
$r$ .... ... ... .... cylinder radius in m
$\theta$.... ... ... ..... radial angle in rad
$z$ .... ... ... .... cylinder length in m
$x_0, y_0, z_0$...... coordinates of defect origin.
$V_\omega$.... ... .... .. volume of defect region $\omega$ in m$^{-3}$
$Q$ .... .... .... .. hydrogen production term in mol m$^{-3}$ s$^{-1}$
$k$.... .... .... ... hydrogen reaction coefficient in mol m$^{-3}$ s$^{-1}$
$T_{(t)}, T^*_{(t)}$.... .... time solution terms
$R_{(r)}$.... ... ... ... radial solution term
$\Theta_{(\theta)}$.... ... ... .. angular solution term
$Z_{(z)}$.... ... ... ... length solution term
$n, m, l$... ... .. indici for summation
$V_m$.... ... ... ... molar volume of iron ($7.09 \times 10^{-6}$ m$^3$ mol$^{-1}$)
$M_H$.... ... ... ... molar mass of hydrogen ($1.00784$ g·mol$^{-1}$)
$M_{Fe}$.... ... ... . molar mass of iron ($55.845$ g·mol$^{-1}$)

### Physical model and geometry

A hollow cylindrical DN50 sample geometry has been selected with the dimensions: outer radius $r_o = 25$ mm, inner radius $r_i = 21$ mm and length $L = 500$ mm (see Fig. 2). For the purpose of this work it is assumed that the outer surface is impermeable for hydrogen (zero flux conditions), except for a rectangular section of 30 mm length and 10 mm width, which stands for the damaged coating where hydrogen can enter. At the inner wall, hydrogen is allowed to leave the material at a rate which is proportional to the diffusion coefficient in steel. Diffusion of hydrogen away from the defect area was derived from the cylindrical diffusion equation (equation (1)).

$$\frac{\partial c}{\partial t} = \frac{\mathbb{D}}{r} \frac{\partial}{\partial r}\left(r \frac{\partial c}{\partial r}\right) + \frac{\mathbb{D}}{r^2} \frac{\partial^2 c}{\partial \theta^2} + \mathbb{D} \frac{\partial^2 c}{\partial z^2} \tag{1}$$

This diffusion equation can be used for modelling transport in single-phase materials, like many pipeline steels. For multi-phase materials, the more general approach to element diffusion needs to be employed by solving not for the local concentration $c$ but the gradient of the chemical potential $\mu$ (local activity $a$) instead. This case also requires the use of migration coefficients $L$ instead of diffusion coefficients $\mathbb{D}$.

### Analytical solution

An explicit solution for equation (1) over the whole cylinder geometry $\Omega$ was derived via the separation of variables ($c_{(t,r,\theta,z)} = T_{(t)} R_{(r)} \Theta_{(\theta)} Z_{(z)}$). This approach has been chosen over standard numerical approaches since analytical solutions allow to quickly alter geometrical and/or material parameters, which would otherwise require significantly more time by using numerical solvers. Because the boundary conditions at the outer surface (constant flux and/or saturation kinetics) have a discontinuity at the edge of the defect area, a minor alteration was introduced. Instead of modelling an inflow of hydrogen through the outer boundary, the entire outer surface was modelled as impermeable and a small volume inside the geometry underneath the defect area, denoted as $\omega$, was attributed with a source term $Q$ (see equation (2)). The source term then mimics the studied cases, set by the three boundary conditions for the defect area, no hydrogen ingress $c_h$, constant hydrogen uptake $c_f$ and kinetically controlled saturation $c_s$ up to a given concentration limit $c_\infty$. Technically, this means that hydrogen appears directly underneath the surface within this finite volume ($\omega \subseteq \Omega$), instead of entering the geometry through the surface. However, because the thickness of this volume was set to 10% of the cylinder wall thickness ($\delta_r = 0.1(r_o - r_i)$), this approximation still stands in good agreement with experimental conditions, whilst avoiding the need to switch back to numeric solutions.

$$\frac{\partial c}{\partial t} = \underbrace{\frac{\mathbb{D}}{r} \frac{\partial}{\partial r}\left(r \frac{\partial c}{\partial r}\right) + \frac{\mathbb{D}}{r^2} \frac{\partial^2 c}{\partial \theta^2} + \mathbb{D} \frac{\partial^2 c}{\partial z^2}}_{\text{diffusion}} + \underbrace{Q_{(r,\theta,z)}}_{\text{source term}} \tag{2}$$

Whilst the derivation of the partial solutions for $T_{(t)}$, $R_{(r)}$, $\Theta_{(\theta)}$ and $Z_{(z)}$ follow standard mathematical procedures, the equations are rather long which is why we only report the solutions in the main manuscript (equations (3)–(5)). For a detailed derivation, the reader is referred to the supplementary material of this work. Three different solutions were obtained, representing the homogeneous solution with diffusion only ($c_h$, $Q = 0$), the solution with a constant hydrogen production rate ($c_f$, $Q = k$) and the solution for kinetic saturation ($c_s$, $Q = k \frac{c_\infty - c_s}{c_\infty}$).

$$c_h = c_0 + \sum_{m=0}^{\infty} Z_{m(z)} \sum_{n=0}^{\infty} \Theta_{n(\theta)} \sum_{l=1}^{\infty} R_{nl(r)} T_{nml(t)} \tag{3}$$

$$c_f = c_0 + \sum_{m=0}^{\infty} Z_{m(z)} \sum_{n=0}^{\infty} \Theta_{n(\theta)} \sum_{l=1}^{\infty} R_{nl(r)} T^*_{nml(t)} \tag{4}$$

$$c_{s(t+\Delta t)} = c_{s(t)} + k\left(1 - \frac{c_{s(t)}}{c_\infty}\right)\Delta t \tag{5}$$

To avoid confusion between different units, all variables were converted to SI units for the calculations. The explicit solutions were plotted in Matlab (The MathWorks Inc., USA). The maximum index of the individual sums in the partial solutions $n$, $m$ and $l$ depend on the size of the geometry $\Omega$ and the defect domain $\omega$ along the corresponding coordinate $r$, $\theta$, $z$. Typical indici values for the geometry in this study are $n_{max} = 80$, $m_{max} = 250$, $l_{max} = 150$.
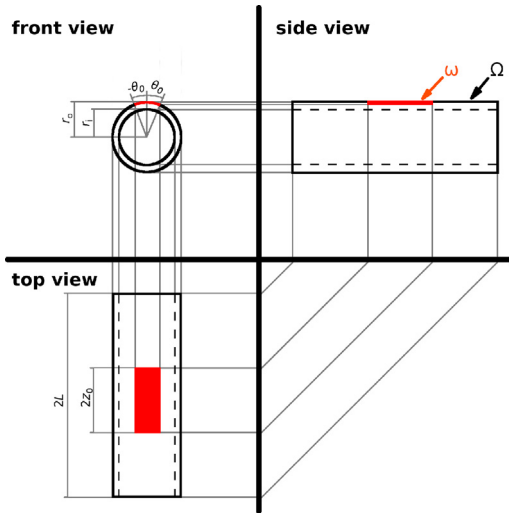
**Fig. 2 – Multiview orthographic projection of the tube geometry with defect area, used throughout this study. The dimensions of the entire simulation domain $\Omega = [r_i, r_o] \times [-\pi, \pi] \times [-L, L]$ as well as for the defect region $\omega = [r_o - \delta_r, r_o] \times [-\theta_0, \theta_0] \times [-z_0, z_0]$ (marked in red) are given.**

*Graphical representation*

Results are plotted as concentration over time for a given measurement position or via contour plots of the local hydrogen concentration as the colour axis. This allows a pairwise analysis of the interaction between simulation parameters $(t, r, \theta, z, \mathbb{D}, k)$ on the local hydrogen concentration $c$. Unless stated otherwise, all concentrations are converted to ppm hydrogen by weight $\beta_H$ (ppm.wt H, equation (6)). At the beginning of the simulation, the sample is assumed to contain a small amount of 0.018 ppm.wt H.

$$\beta_H = \frac{cM_H}{cM_H + \frac{M_{Fe}}{V_m}} \times 10^6 \tag{6}$$

## Experimental set-up

For measurement of the hydrogen diffusion through a cylindrical geometry, a DN 50 pipeline steel with 4 mm wall thickness and an external polyethylene coating was used. The composition of the steel was given as follows: 0.11 wt% C, 0.51 wt% Mn, 0.014 wt% P, 0.008 wt% S and 0.033 wt% Cu. The hydrogen loading was performed at a coating defect according to Fig. 2 with $z_o$ of 15 mm and $\theta_0$ of 11.5°. The coating defect with a surface of 3 cm$^2$ was buried in quartz sand saturated with artificial soil solution as described in [20]. This corresponds to an artificial soil condition with a non-film forming electrolyte. A cathodic current density of 1 A m$^{-2}$ was applied to the coating defect. At positions $z$ of 38 mm, 162 mm and 455 mm, a hole was drilled through the PE coating and a PMMA tube was glued to the exposed steel surface. The tube was filled with a solution of 0.1 M NaOH and 1 mM NaCl and closed

by means of a plug to prevent evaporation. An AgCl coated silver wire was permanently introduced into the solution. The voltage between the pipe wall and the silver wire was measured in 30 min intervals. These potential values were converted to the standard hydrogen electrode reference (SHE) potential.

## Results and discussion

The accuracy of the simulations have been verified by comparing to two well-documented cases for diffusion. The first case corresponds to the diffusion along a semi-infinite rod with a constant concentration on one side, which can be calculated with relative ease by the error function (equation (7)). This has been approximated in the model by setting the inner radius close to zero and setting the geometry of the defect region $\omega$ to a thin slice of the rod. Consequently, the loss of hydrogen through the inner cylinder wall also becomes close to zero because the inner surface area scales linearly with the radius. Constant concentration in the defect region has been mimicked by the solution for kinetic saturation $c_s$ and using a high kinetic rate coefficient ($k = 100$). The second comparison was against the free diffusion from a point source in a flat plate. This case can be approximated by setting the outer radius to a large value ($r_o = 500$ mm) and the size of the defect area $\omega$ to be very small. A small defect area relative to the cylinder thickness means that the diffusion of hydrogen through the inner wall, which would be the bottom side of the plate, is again very small. The diffusion from a point source (Dirac function) can then be described by a Gaussian function as shown in equation (8). In both cases, the absolute difference between the simulation and the analytical solution was always below 0.478 ppm.wt H and 0.196 ppm.wt H respectively, given an absolute error which is always below 5%. Although the developed model can only be used for an approximation to these cases, the obtained accuracy from this comparison was deemed to describe the diffusion process reasonably well.

$$c_{(t,r,\theta,z)}^{rod} = c_0 + (c_\infty - c_0)\, \mathrm{erf}\left(\frac{z}{\sqrt{4\mathbb{D}t}}\right) \tag{7}$$

$$c_{(t,r,\theta,z)}^{plate} = c_0 + \frac{(c_\infty - c_0)V_\omega}{(4\mathbb{D}t)^{\frac{3}{2}}} e^{-\frac{(x-x_0)^2 + (y-y_0)^2 + (z-z_0)^2}{4\mathbb{D}t}} \tag{8}$$

*Diffusion only and constant hydrogen production*

Fig. 3 shows the local hydrogen concentration for the homogeneous solution $c_h$ as well as for the solution with constant hydrogen production $c_f$ at specific measurement positions. For the diffusion only case ($c_h$, $Q = 0$), the initial concentration was set to 10 ppm.wt H in the defect region. In an experimental setting, this would correspond to the distribution of hydrogen in a sample, which has experienced a sudden uptake of hydrogen, either via exposure to a cathodic current pulse or a sample which very quickly forms a protective film, blocking
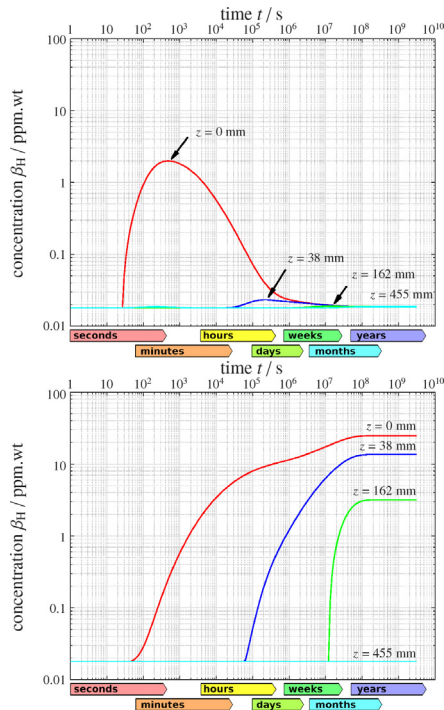
**Fig. 3 − Change of local hydrogen concentration in a DN50 tube geometry over a time span from 1 s up to 100 years. The z-positions are measured from the origin of the defect volume $\omega$ at a quarter thickness from the surface. The initial hydrogen concentration was 0.018 ppm.wt. Hydrogen transport was calculated for only diffusion ($\mathbb{D} = 10^{-9}$ m² s⁻¹) without additional hydrogen uptake and a starting hydrogen concentration of 10 ppm.wt in the defect volume (top) as well as for the initial hydrogen concentration in the defect volume and a constant hydrogen production/inflow of 1 A m⁻² (bottom).**

further hydrogen ingress. As time progresses, a rise in the hydrogen concentration directly underneath the defect center can be seen after a few seconds, which slowly vanishes after approximately 1 day. Very small changes in the local hydrogen concentration can be seen further away from the defect center but the total amount of hydrogen remains very small.

For conditions of constant hydrogen production/ingress ($c_f$, $Q = $ const.), a rise of the local hydrogen concentration can be seen for nearly all measurement positions. Whilst underneath the defect origin, this increase was observed between 1 and 2 min, distances further away experience this rise much later, at a timescale of several days or even months, which is to be expected from a diffusion behaviour. No increase of the local hydrogen concentration was seen for the farthest position in the simulations which is due to an insufficient amount of hydrogen being produced in the defect region. For all other measurement positions, the hydrogen local concentration seems to level off after some time. This is due to the fact that whilst hydrogen is produced at a constant rate, the flux of hydrogen ($j_H = \mathbb{D} \times \nabla c$) increases as well. At some time, the local hydrogen concentration becomes so large, that the flux

equals the amount of new hydrogen being produced ($Q = j_H$), which manifests itself in a steady value of the local hydrogen concentration. Mathematically, it would be expected that the curve increases again once the entire geometry has been filled but simulations have shown that this lies beyond a timescale of 100 years. Even longer time periods were not relevant for this study since a material lifetime of 100 years was assumed for this study. It should be noted that a constant uptake of hydrogen can only be achieved under conditions where the uptake rate is rather small [19,21,22]. If this is not the case, the rate of hydrogen entering the geometry continuously decreases (e.g. decrease of Faraday efficiency in an electrochemical reaction), which has also been shown by other groups [12,23,24]. Both solutions $c_h$ and $c_f$ are indeed extreme cases for the hydrogen uptake. However, they are still relevant to predict either the free diffusion or the constant loading at low uptake rates or the situation at the early stages of hydrogen accumulation. In all three cases, the efficiency of hydrogen uptake compared to the total amount of hydrogen produced, which includes losses due to hydrogen evolution at the surface, is close to 100% [12].

*Hydrogen concentration along pipeline*

Given a saturation limit for the local hydrogen concentration near the surface ($c_\infty = 10$ ppm.wt H in this study), the hydrogen uptake must decrease with time, which is represented by the solution for kinetic loading $c_s$. Fig. 4 shows the change of the local hydrogen concentration as a function of distance from the defect origin at a depth of 1 mm underneath the outer surface, corresponding to a quarter thickness. Due to the implicit solution on the time axis, the number of points became very large and exceeded the memory limit of the programme. Hence, the calculations of kinetic saturation were limited to a time frame of 1 month, still providing details on the evolution of the local hydrogen concentration. The experimental results from electrochemical measurements are shown in Fig. 4a. A significant drop of the potential can be observed in the experiments between 1 and 3 days for the position closest to the defect center, whilst the simulations predict a change in hydrogen concentration after 5−6 days. The reason for this discrepancy can be manifold and may be attributed to a slightly different diffusion coefficient in the material compared to the simulations, the width of the sensor in the measurement position in the experiments as well as the possibility that small amounts of hydrogen accumulated near the sensor because the coating had to be removed for the detection of hydrogen. Furthermore, the boundary conditions from section 2.1 (zero flux through outer surface, regular diffusion through inner surface) are idealised assumptions which may also deviate from the experimental conditions. However, despite the number of potentially uncertain factors in the complex set-up and the fact that modelling parameters were taken from independent literature sources, a good agreement between simulations and experiments was achieved.

The contour plot of the hydrogen concentration in Fig. 4 clearly shows that the total amount of hydrogen does not exceed the saturation level and therefore the efficiency of the hydrogen uptake must decrease steadily. Whilst rather little
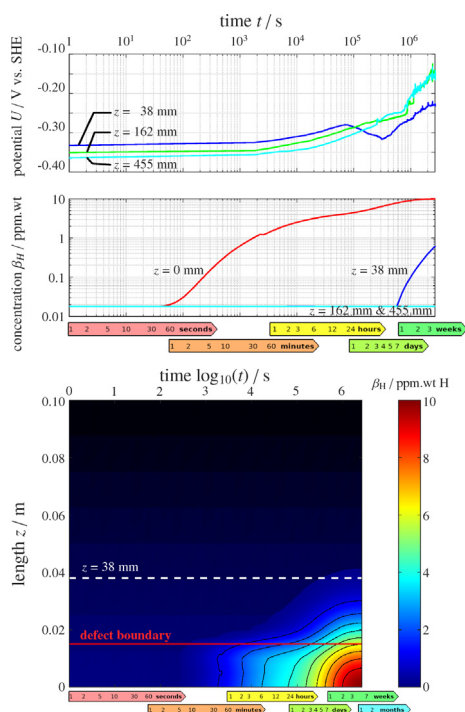
**Fig. 4** – Change of local hydrogen concentration in a DN50 tube geometry with time. The z-positions are measured from the origin of the defect volume $\omega$ at a quarter thickness from the surface. The change of potential vs. standard hydrogen electrode (SHE) from the experiments (top), simulation results at selected measurement positions z over time (middle) and change of local hydrogen concentration along the tube length (bottom) are shown. Simulations were carried out with a kinetic saturation term, (solution for $c_s$) and a hydrogen production/inflow of 1 A m$^{-2}$. The initial hydrogen concentration in the simulations was 0.018 ppm.wt and a saturation value of $c_\infty = 10$ ppm.wt.

changes in the local hydrogen concentration can be seen for less than 1 h, the hydrogen concentration slowly rises, yet seems to stay localised near the defect region. This is in agreement with the expected diffusion length for typical diffusion coefficients ($\mathbb{D} = 10^{-9}$ m$^2$ s$^{-1}$), reported in literature [17,18,25−27].

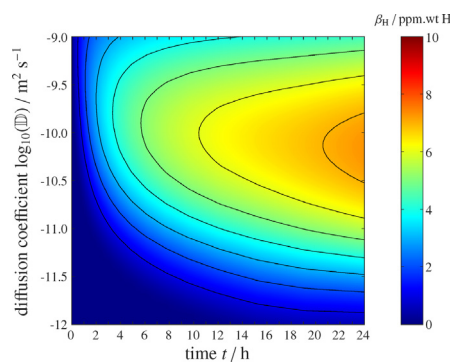*Variation of effective hydrogen diffusion coefficient*

The correlation of the local hydrogen concentration with the effective diffusion coefficient $\mathbb{D}$ is shown in Fig. 5 and has gained a longstanding interest in the scientific community [19,25,28−30]. Due to changes in microstructure, the amount of trap sites which hamper hydrogen in its mobility will ultimately affect the local hydrogen transport. Thermal desorption studies are often used to characterise the trapping behaviour of hydrogen and to calculate the effective diffusion coefficient of hydrogen, according to the theory of Oriani [28,29,31]. Within this study, the hydrogen diffusion

coefficient is treated as an input parameter, which has been varied in a range typically reported for pipeline steels [17,18]. Since rather small changes have been seen in previous figures for positions further away from the defect center, the local hydrogen concentration was calculated for a position underneath the defect region $\omega$, at a quarter thickness of the cylinder wall.
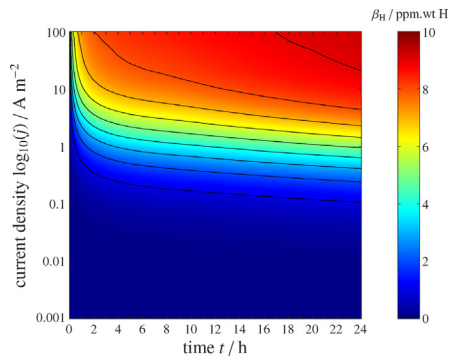
The local hydrogen concentration in Fig. 5 exhibits a maximum at an effective diffusion coefficient of $\approx 10^{-10}$ m$^2$ s$^{-1}$. This is due to the fact that for slower diffusion, the hydrogen has not yet arrived at the observed position and hence the increase of the local hydrogen concentration is delayed. Obviously, this time delay is shorter, the closer the position is to the defect origin. For higher diffusion coefficients, hydrogen is diffusing faster than it's being produced in the defect region and hence the overall concentration profile appears to be flatter. It should be noted that the increase of local hydrogen diffusion starts earlier for faster diffusivities, as it would be expected from a typical diffusion behaviour. From a practical perspective, this means that intermediate diffusion values can be dangerous because they lead to an increased concentration of hydrogen at some distance from the defect area, which may further accelerate mechanical damage to the material by enhancing crack propagation or lowering the fatigue performance [30]. At extremely low diffusivities, the hydrogen ingress becomes strongly localised whilst for fast diffusion, the local hydrogen concentrations may be too small to cause significant changes to the mechanical performance of the material.

*Variation of cathodic corrosion protection current density*

The change of the local hydrogen concentration as a function of the hydrogen production/uptake rate k, is shown in Fig. 6. Clearly, the higher the hydrogen ingress, the quicker the geometry reaches the saturation level. Whilst this behaviour



**Fig. 5** – Change of local hydrogen concentration in a DN50 tube geometry over time for a typical range of effective hydrogen diffusion coefficients $\mathbb{D}$. The position is at the origin of the defect volume $\omega$ (z = 0 mm) at a quarter thickness from the surface. Simulations were carried out with a kinetic saturation term (solution for $c_s$) and a hydrogen production/inflow of 1 A m$^{-2}$. The initial hydrogen concentration in the simulations was 0.018 ppm.wt and a saturation value of $c_\infty = 10$ ppm.wt.

Fig. 6 − Change of local hydrogen concentration in a DN50 tube geometry over time for different hydrogen production/inflow $j$. The position is at the origin of the defect volume $\omega$ ($z = 0$ mm) at a quarter thickness from the surface. Simulations were carried out with an effective hydrogen diffusion coefficient of $10^{-9}$ m$^2$ s$^{-1}$ and a kinetic saturation term (solution for $c_s$). The initial hydrogen concentration in the simulations was 0.018 ppm.wt and a saturation value of $c_\infty = 10$ ppm.wt.

Fig. 7 − Change of local hydrogen concentration in a DN50 tube geometry for a fixed time and position as a function of effective hydrogen diffusion coefficient $\mathbb{D}$ and hydrogen production/uptake $j$. Simulations were carried out for $t = 10$ years and position at the origin of the defect volume ($z = 0$ mm) in quarter thickness from the surface, using a kinetic saturation term (solution for $c_s$). The initial hydrogen concentration in the simulations was 0.018 ppm.wt and a saturation value of $c_\infty = 10$ ppm.wt.
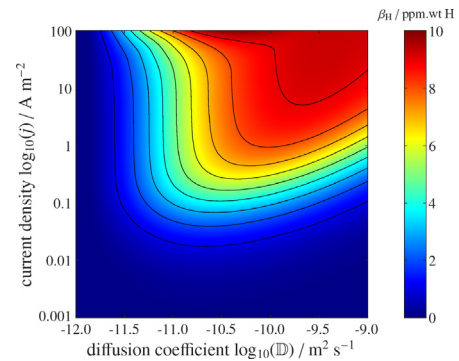
may intuitively be clear to the reader, it should be stressed that a quantification becomes important because the coefficient $k$ also represents kinetic barriers which may hamper the uptake of hydrogen in the material. The change of the uptake rate thus becomes very important to determine the stability of a surface against excessive hydrogen uptake.

In Fig. 6, it can be seen that an uptake rate corresponding to a current density of 1 A m$^{-2}$ leads to a significant increase of the local hydrogen concentration 1 mm underneath the defect area after approximately 1 h, whilst lower uptake rates show similar concentrations at significantly longer times. Current densities below 0.1 A m$^{-2}$ don't show increased amounts of hydrogen within the first 24 h, which also indicates that the solutions for constant flux $c_f$ and kinetic saturation $c_s$ are expected to provide similar results under these conditions.

### Variation of effective hydrogen diffusion and cathodic corrosion protection current density

The combination of diffusion coefficient $\mathbb{D}$ and kinetic hydrogen uptake rate $k$ is shown in Fig. 7. This graph represents the hydrogen concentration at a single position for a given (fixed) time and shows combinations of hydrogen ingress and diffusivity, that lead to a significant increase of the local hydrogen concentration.

As it can be seen in Fig. 7, hydrogen accumulates for high uptake rates $k$, corrosion current densities $j$ as well as for intermediate values for the diffusion coefficient $\mathbb{D}$. If the diffusivity is smaller, hydrogen becomes very localised near the defect area and does not spread further away into the material. When the diffusivity is quite high, the distribution of hydrogen becomes very shallow. It can be seen from the graph, that this depends on the combination of effective hydrogen diffusivity in the material and the hydrogen uptake rate, which does not seem to follow a simple, linear law.

Especially for extremely high hydrogen uptake rates, it can be seen that the range of high concentrations also extends to lower diffusivities, which is caused by a quick saturation of the defect area which then acts as a source with a constant hydrogen concentration that slowly begins to fill the rest of the geometry.

## Conclusions

An analytical model to predict the diffusion of hydrogen in a cylindrical geometry has been developed. The geometry is a laboratory-scale model of a pipeline with a coating defect at the surface, which exposes the material to potential hydrogen ingress due to cathodic protection. The model has been tested against two well-documented cases in literature such as one-dimensional diffusion along a semi-infinite rod with constant concentration at the surface and diffusion of a point source across a plate. The absolute error between the analytical model and both cases was always below 5%, although these test cases can only be approximated by the model.

Two extreme cases, showing no hydrogen uptake ($c_h$, $Q = 0$) and constant hydrogen uptake ($c_f$, $Q = $ const.) as well as the intermediate case of kinetic controlled hydrogen uptake $c_s$ up to a saturation level $c_\infty$ were studied. If only diffusion without any additional hydrogen uptake occurs, changes of the hydrogen concentration mostly affect the region directly next to the defect area within a timeframe between minutes and several hours. Constant hydrogen uptake reaches much farther away, up to several centimeters from the defect area and in timeframes between a few hours and several weeks. Due to the reported losses of the hydrogen uptake efficiency at high current densities in experimental works, constant hydrogen uptake may, however, only be feasible for low uptake rates (e.g. low corrosion protection current densities)

where the local hydrogen concentrations remain well below the hydrogen solubility limit in the material or in the case of fast hydrogen diffusion away from the defect region. Modelling hydrogen diffusion with kinetic saturation $c_s$ appears to be the most suitable solution for the practical case, which also includes the drop in efficiency of hydrogen uptake when the defect area begins to reach local saturation, as frequently described in literature.

Simulation results agree reasonably well with the experiments, given potential discrepancies (e.g. sensor position) and uncertainties (e.g. effective hydrogen diffusivity and initial hydrogen concentration) in the parameters between the simulations and the measurements. Whilst the entire parameter space $(t,r,\theta,z,\mathbb{D},k)$ cannot be visualised in a two-dimensional plot, binary interactions between simulation parameters have been shown to visualise conditions which may lead to a maximum accumulation of hydrogen. Results have also shown that the dependency between relevant parameters such as effective hydrogen diffusion in the material and kinetic hydrogen uptake rate through the defect region, leading to these critical conditions is nonlinear and requires further investigation.

## Declaration of competing interest

The authors declare that they have no known competing financial interests or personal relationships that could have appeared to influence the work reported in this paper.

## Acknowledgements

## Appendix A. Supplementary data

Supplementary data to this article can be found online at https://doi.org/10.1016/j.ijhydene.2023.05.181.

REFERENCES

[1] Angst U, Büchler M, Martin B, Schöneich H-G, Haynes G, Leeds S, Kajiyama F. Cathodic protection of soil buried steel pipelines - a critical discussion of protection criteria and threshold values. Mater Corros 2016;67:1135–42.

[2] Frankel G, Samaniego A, Birbilis N. Evolution of hydrogen at dissolving magnesium surfaces. Corrosion Sci 2013;70:104–11.

[3] Tlili M, Benamor M, Gabrielli C, Perrot H, Tribollet B. Influence of the interfacial pH on electrochemical CaCO$_3$ precipitation. J Electrochem Soc 2003;150:765–71.

[4] Auinger M, Katsounaros I, Meier J, Klemm S, Biedermann P, Topalov A, Rohwerder M, Mayrhofer K. Near-surface ion distribution and buffer effects during electrochemical reactions. Phys Chem Chem Phys 2011;13:16384–94.

[5] Freiman L, Strizhevskii I, Yunovich M. Passivation of iron in soil with cathodic protection. Protect Met 1988;104:78–80.

[6] Leeds J. Cathodic-generated film protects pipe surface - part 1. Pipe Line Ind 1992;4:39–45.

[7] Peabody A. In: Bianchetti R, editor. Control of pipeline corrosion, 2. Houston, Texas: NACE; 2001, 70027.

[8] Büchler M. On the mechanism of cathodic protection and its implications on criteria including AC and DC interference conditions. Corrosion 2020;76:451–63.

[9] Büchler M. A new perspective on cathodic protection criteria promotes discussion. Mater Perform 2015;54:44–8.

[10] Pourbaix M, editor. Atlas of electrochemical equilibria in aqueous solutions. 1st ed. Houston, Texas, USA: National Association of Corrosion Engineers; 1974.

[11] Schwerdtfeger W, McDorman O. Potential and current requirements for the cathodic protection of steel in soils. ournal of Research of the National Bureau of Standards 1951;47:104–12.

[12] Grobe S, Prinz W, Schöneich H, Wingeder J. Einfluss sulfatreduzierender Bakterien auf den kathodischen Korrosionsschutz. Mater Corros 1996;47:413–24.

[13] Barbalat M, Lanarde L, Caron D, Meyer M, Vittonato J, Castillon F, Fontaine S, Refait P. Electrochemical study of the corrosion rate of carbon steel in soil: evolution with time and determination of residual corrosion rates under cathodic protection. Corrosion Sci 2012;55:246–53.

[14] Büchler M. Alternating current corrosion of cathodically protected pipelines: discussion of the involved processes and their consequences on the critical interference values. Mater Corros 2012;63:1181–7.

[15] Kuhn R. Galvanic current on cast iron pipes. Ind Eng Chem 1930;22:335–41.

[16] Parkins R, Zhou S. The stress corrosion cracking of C-Mn steel in CO2-$HCO_3^-$-$CO_3^{2-}$ solutions. I: stress corrosion data. Corrosion Sci 1997;39:175–91.

[17] Juilfs G. Das Diffusionsverhalten von Wasserstoff in einem niedriglegierten Stahl unter Berücksichtigung des Verformungsgrades und der Deckschichtbildung in alkalischen Medien, Ph.D. thesis. Technische Universität Hamburg-Harburg; 2000.

[18] Fallahmohammadi E, Bolzoni F, Fumagalli G, Re G, Benassi G, Lazzari L. Hydrogen diffusion into three metallurgical microstructures of a C-Mn X65 and low alloy F22 sour service steel pipelines. Int J Hydrogen Energy 2014;39:13300–13.

[19] Auinger M. Hydrogen transport in non-ideal crystalline materials. ChemPhysChem 2014;15:2893–902.

[20] Büchler M, Voûte C-H, Stadler F. In: The electrochemical society proceedings series (Ed.), Critical Factors in Localized Corrosion IV, Pennington, NJ; 2003. p. 436–44. https://books.google.co.uk/books/abou/Critical_Factors_in_Localized_Corrosion.html?id=qlWK8IJAPdUC&redir_esc=y. https://books.google.co.uk/books?id=qlWK8IJAPdUC&pg=PA436&source=gbs_toc_r&cad=4#v=onepage&q&f=false.

[21] Sieverts A. Die Aufnahme von Gasen durch Metalle. Z Metallkd 1919;21(2):37–46.

[22] Lewis F. Solubility of hydrogen in metals. Pure Appl Chem 1990;62:2091–6.

[23] Liu Q, Atrens A, Shi Z, Verbeken K, Atrens A. Determination of the hydrogen fugacity during electrolytic charging of steel. Corrosion Sci 2014;87:239–58.

[24] Capelle J, Dmytrakh I, Pluvinage G. Comparative assessment of electrochemical hydrogen adsorption by pipeline. Corrosion Sci 2010;52:1554–9.

[25] Johnson H, Kumnick A, Quick N. Hydrogen trapping. In: Effect of hydrogen on behaviour of materials; 1975. p. 349—54.

[26] Hirth J. Effects of hydrogen on the properties of iron and steel. Metall Trans A 1980;11:861—90.

[27] Riecke E, Johnen B, Grabke H. Effects of alloying elements on corrosion and hydrogen uptake of iron in sulfuric acid part i: permeation, diffusion and solubility of hydrogen in binary iron alloys. Mater Corros 1985;36:435—41.

[28] Oriani R. The diffusion and trapping of hydrogen in steel. Acta Metall 1970;18:147—57.

[29] Kirchheim R. Solubility, diffusivity and trapping of hydrogen in dilute alloys. deformed and amorphous metals-ii. Acta Metall 1982;30:1069—78.

[30] Fukai Y, Sugimoto H. Diffusion of hydrogen in metals. Adv Phys 1985;34:263—326.

[31] Kirchheim R. Hydrogen solubility and diffusivity in defective and amorphous metals. Prog Mater Sci 1988;32:261—325.

## Appendix A. Mathematical Derivation of Solution

The entire derivation of the general analytical solution is shown for the homogeneous solution $c_h$. The particulate solutions for constant flux $c_f$ and kinetic saturation $c_s$ are special extensions of the homogeneous solution and hence only the modifications will be shown in the corresponding subsections. The following general definitions apply for all subsections:

- The coordinate system $(r, \theta, z)$ runs in radial direction through the center of the defect area and spans the entire domain of the hollow cylinder $\Omega = [r_i, r_o] \times [-\pi, \pi] \times [-L, L]$.

- The defect volume where hydrogen is produced in the simulations has the dimensions $\omega = [r_o - \delta_r, r_o] \times [-\theta_0, \theta_0] \times [-z_0, z_0]$.

- The hydrogen production rate depends only on the kinetic term $Q$. No additional limitations from transport outside of the cylinder geometry were considered.

- Based on the problem statement in the main manuscript, we assume that the initial hydrogen concentration in the pipe is uniform and constant at $c_0 = 0.018$ ppm.wt H

### Appendix A.1. Homogeneous Solution $c_h$

We begin with the cylindrical diffusion equation (equation 1) and separate the variables $c_{(t,r,\theta,z)} = T_{(t)}R_{(r)}\Theta_{(\theta)}Z_{(z)}$ thus isolating the time-dependent variable first. For the equation to be fulfilled, both terms must be equal to a (real number) constant $\alpha$.

$$\frac{1}{\mathbb{D}T}\frac{\partial T}{\partial t} = \frac{1}{rR}\frac{\partial}{\partial r}\left(r\frac{\partial R}{\partial r}\right) + \frac{1}{r^2\Theta}\frac{\partial^2\Theta}{\partial\theta^2} + \frac{1}{Z}\frac{\partial^2 Z}{\partial z^2} = \alpha \quad (\alpha \in \mathbb{R})$$
(A.1)

To keep the expressions in equation A.1 and all further equations rather easy to the eye, we write for the functions $T_{(t)}, R_{(r)}, \Theta_{(\theta)}$ and $Z_{(z)}$ only the main expressions $T, R, \Theta$ and $Z$. This equation can now subsequently be solved by one variable after the other.

In order to derive the *time dependent solution* $T_{(t)}$ from equation A.1, we need to set the time dependent part of the equation equal to the constant $\alpha$. One quickly obtains the solution.

$$T_{(t)} = T_0 e^{\alpha \mathbb{D}t} \quad (\alpha \in \mathbb{R}, T_0 \in \mathbb{R}_0^+)$$
(A.2)

To calculate the *solution for the cylinder length* $Z_{(z)}$, one isolates the corresponding variable fom the middle and right-hand side of equation A.1, defining another constant $\beta$.

$$\frac{1}{rR}\frac{\partial}{\partial r}\left(r\frac{\partial R}{\partial r}\right) + \frac{1}{r^2\Theta}\frac{\partial^2\Theta}{\partial\theta^2} - \alpha = -\frac{1}{Z}\frac{\partial^2 Z}{\partial z^2} = \beta \quad (\beta \in \mathbb{R})$$
(A.3)

When examining the two terms on the right-hand side and by multiplying this equation with $-Z$, we again come to a solution for the corresponding variable with relative ease.

$$Z_{(z)} = A \sin\left(\sqrt{\beta}z\right) + B \cos\left(\sqrt{\beta}z\right) \quad (\beta, A, B \in \mathbb{R}) \quad (A.4)$$

To obtain the *solution for the angle* $\Theta_{(\theta)}$, we start with the relationship in equation A.3 and modify to obtain the reduced version which only contains $\Theta$ and $R$. We can now rewrite this equation to further separate the expressions with variables $\theta$ and $r$ from each other.

$$\frac{r}{R}\frac{\partial}{\partial r}\left(r\frac{\partial R}{\partial r}\right) - r^2(\alpha + \beta) = -\frac{1}{\Theta}\frac{\partial^2\Theta}{\partial\theta^2} = \gamma \quad (\gamma \in \mathbb{R})$$
(A.5)

Only the two terms on the right-hand side of equation A.5 contain $\theta$ and we again get a solution very quickly which describes the angular dependency of the concentration distribution.

$$\Theta_{(\theta)} = C \sin\left(\sqrt{\gamma}\theta\right) + D \cos\left(\sqrt{\gamma}\theta\right) \quad (\gamma, C, D \in \mathbb{R}) \quad (A.6)$$

The *solution for the radial term* $R_{(r)}$ is the most complex part. From equation A.5 we obtain

$$\frac{r}{R}\frac{\partial}{\partial r}\left(r\frac{\partial R}{\partial r}\right) - (\alpha + \beta)r^2 = \gamma \quad (\alpha, \beta, \gamma \in \mathbb{R}) \quad (A.7)$$

This equation can further be modified into a known form of an ordinary diffusion equation which has the shape of a Bessel-type diffusion equation ($x^2 y'' + xy' + \left(x^2 + \nu\right) = 0$). We substitute for the radius $\rho = i\sqrt{\alpha + \beta} \cdot r$ and need to consider the inner derivative of the function $R_{(r)}$. For the sake of simplicity, we write $R'$ for the first derivative and $R''$ for the second derivative and obtain

$$\rho^2 R''_{(\rho)} + \rho R'_{(\rho)} + \left(\rho^2 - \gamma\right) R_{(\rho)} = 0 \quad (A.8)$$

The solutions for equation A.8 are a linear combination of Bessel functions of first kind ($J$) and second kind ($Y$). These can be written as follows

$$R_{(r)} = EJ_{\left(\sqrt{\gamma},\, i\sqrt{\alpha+\beta}\; r\right)} + FY_{\left(\sqrt{\gamma},\, i\sqrt{\alpha+\beta}\; r\right)} \quad (\alpha,\beta,\gamma,E,F \in \mathbb{R}) \tag{A.9}$$

An explicit analytical (and finite) expression for these functions does not exist. However, both types can be approximated by a series of polynomials. Modern programmes do contain these functions in sufficient numerical accuracy. In order to obtain the *fundamental solution for the cylindrical diffusion equation*, we now must combine the partial solutions for every variable $c_{(t,r,\theta,z)} = T_{(t)}R_{(r)}\Theta_{(\theta)}Z_{(z)}$, thus combining equations A.2, A.4, A.6 and A.9. Given the complexity of the combined term, it may seem reasonable to first consider the boundary conditions for each equation. This will be addressed in the next subsections. Based on the description from sections 2.3 and Appendix A, we assume that the initial hydrogen concentration in the pipe is uniform and constant at 0.018 ppm.wt H.

*Appendix A.2. Particulate Solution for Constant Flux $c_f$*

Assuming an extreme theoretical scenario for hydrogen accumulation, where the uptake efficiency is always 100%, hydrogen will be produced at a constant rate in the area where the coating is damaged (i.e. the volume $\omega$ in figure 2). Assuming the hydrogen uptake is caused by an electrochemical process, such as cathodic protection, the molar rate can be calculated from Faraday's law, leading to the following definition of initial conditions $c(t = 0, r, \theta, z)$ and source term $Q$.

$$c(t = 0, r, \theta, z) = c_0 \in \mathbb{R}_0^+$$

$$Q = \begin{cases} \frac{j}{F\delta_r}\frac{1}{1-\frac{\delta_r}{2r_0}} & (r,\theta,z) \in \omega \\ 0 & \text{everywhere else} \end{cases}$$

For the determination of the *angular dependency* $\Theta_{(\theta)}$, $\theta$ will be varied in the interval $(-\pi, \pi)$. Considering the width of the defect side to range from $-\theta_0$ to $+\theta_0$, we do get the follwing definition of the angular dependency.

$$\Theta_{(\theta)} = \begin{cases} 1 & \theta \in [-\theta_0, \theta_0] \subset \omega \\ 0 & \text{everywhere else} \end{cases}$$

This function can be approximated via a Fourier-Cosine series. Since $\Theta_{(\theta)}$ is an even function ($\Theta_{(-\theta)} = \Theta_{(\theta)}$), all the sine-terms are zero and we remain with a Fourier-Cosine-Series of a pulse signal, which has the following type:

$$\Theta_{(\theta)} \approx \sum_{n=0}^{\infty} \Theta_{n(\theta)} = \frac{\theta_0}{\pi} + \sum_{n=1}^{\infty} \frac{2}{n\pi} sin(n\theta_0) cos(n\theta) \tag{A.10}$$

In particular, when comparing this to the general solution for $\Theta_{(\theta)}$ (equation A.6), we can see that only the cosine-terms remain. Thus we know that $C = 0$ and $\gamma = n^2$.

The *cylinder length $Z_{(z)}$* solution term is similar to the angular dependency and so the equations are of similar form.

$$Z_{(z)} = \begin{cases} 1 & z \in [-z_0, z_0] \subset \omega \\ 0 & \text{everywhere else} \end{cases}$$

$$Z_{(z)} \approx \sum_{m=0}^{\infty} Z_{m(z)} = \frac{z_0}{L} + \sum_{m=1}^{\infty} \frac{2}{m\pi} sin\left(m\pi\frac{z_0}{L}\right) cos\left(m\pi\frac{z}{L}\right) \tag{A.11}$$

When comparing the variables to equation A.4, we can conclude that $A = 0$ and $\beta = \frac{m^2\pi^2}{L^2}$.

For the *radial dependency $R_{(r)}$* in the problem statement, we assumed an extreme scenario for hydrogen accumulation and hence need to insert insulating boundary condition for hydrogen transport at the outer surface ($\partial_r R_{(r_o)} = 0$). The radial term itself follows the form

$$R_{(r)} = \begin{cases} 1 & r \in [r_o - \delta_r, r_o] \subset \omega \\ 0 & \text{everywhere else} \end{cases}$$

The solution for $R$ has (again) the form of a pulse, which can be approximated by a Fourier-Bessel series. Without loss of generality, we can show that the prefactor for the Bessel functions of second kind $Y$ has to be zero, since $Y(n, 0) \to -\infty$. Even though inner pipe radii cannot be zero, we could potentially assume any pipe size and inner radii where one can proof by induction that as $r_i \to 0$, the coefficient $F$ in equation A.9 approaches zero. We then get for the solution

$$R_{n.(r)} \approx \sum_{l=1}^{\infty} e_{nl}\, J\left(n, \lambda_{nl}\frac{r}{r_o}\right) \tag{A.12}$$

$$\text{with}\quad e_{nl} = \frac{\int_{r_i}^{r_o} rR_{(r)}J(n, \lambda_{nl}\frac{r}{r_o})dr}{\int_{r_i}^{r_o} rJ^2(n, \lambda_{nl}\frac{r}{r_o})dr} \tag{A.13}$$

where $\lambda_{nl}$ is the $l^{th}$ zero of the derivative of the Bessel function $J(n, r)$. The $\lambda_{nl}$ only become equidistant for very large radii but all values are tabulated in literature or can be calculated via Newton's method for approximating zeros. Moreover, we do get a new approximation

for every order parameter $n$. This makes a combination of all the partial solutions more complex because of the relationship between $\alpha, \beta$ and $\gamma$. If we further substitute the variable $\rho = \frac{r}{r_o}$ and develop the step function right from the origin ($r = 0$), we can derive an explicit solution for the coefficient $e_{nl}$ with $\lambda_{nl}$ being the zeros of $J(n, r)$. For the case of $n = 0$, we can solve both integrals for $e_{nl}$ explicitly, leading to

$$e_{0l} = \frac{\frac{1}{\lambda_{0l}} J(1, \lambda_{0l}) - \left(1 - \frac{\delta_r}{r_o}\right) J\left(1, \left(1 - \frac{\delta_r}{r_o}\right)\lambda_{0l}\right)}{\frac{1}{2} J^2(1, \lambda_{0l})} \quad (A.14)$$

We thus get for the solution of the radial term:

$$R_{n(r)} \approx \sum_{l=0}^{\infty} R_{nl(r)} \quad (A.15)$$

with $R_{nl(r)} = \begin{cases} \frac{2}{\lambda_l} \dfrac{J(1,\lambda_l) - \left(1-\frac{\delta_r}{r_o}\right) J\left(1,\left(1-\frac{\delta_r}{r_o}\right)\lambda_l\right)}{J^2(1,\lambda_l)} \, J\left(0, \lambda_l \frac{r}{r_o}\right) & \text{for } n = 0 \\[2em] \dfrac{\int_{r_o-\delta_r}^{r_o} r J(n, \lambda_{nl}\frac{r}{r_o}) dr}{\frac{1}{2} J^2(n+1, \lambda_{nl})} \, J\left(n, \lambda_{nl}\frac{r}{r_o}\right) & n > 0 \ (n \in \mathbb{N}) \end{cases}$

When comparing the variables to equation A.9, the substitution in the Bessel functions and the result for $\beta$, we can conclude that $\alpha = -\left(\frac{\lambda_{nl}^2}{r_o^2} + \frac{m^2\pi^2}{L^2}\right)$. This relationship must be carefully considered for the derivation of the time dependent solution.

The form of the *time dependent solution* $T_{(t)}^*$ has to contain the homogeneous solution ($Q = 0$, equation A.2) and a particulate solution which must match the additional source term $Q$. It should be noted that because $\alpha$ is a function of $n, m$ and $l$, it means that the time dependency is also a function of $n, m$ and $l$. For the particulate solution, we can use the method of the variation of the constant $T_0 \to T_{0(t)}$. Taking the first time derivative, we get

$$\frac{\partial T_{(t)}}{\partial t} = \underbrace{T_{0(t)}\alpha_{nml}\mathbb{D} \, e^{\alpha_{nml}\mathbb{D}t}}_{\text{homogenous solution}} + \underbrace{\frac{\partial T_{0(t)}}{\partial t} e^{\alpha_{nml}\mathbb{D}t}}_{\text{particulate solution}} \quad (A.16)$$

Using the condition, derived at the beginning of this subsection where $Q = \frac{j}{F\delta_r} \frac{1}{1-\frac{\delta_r}{2r_0}}$, we obtain the relationship for the particulate solution.

$$\frac{\partial T_{0(t)}}{\partial t} e^{\alpha_{nml}\mathbb{D}t} = \frac{j}{F\delta_r} \frac{1}{1-\frac{\delta_r}{2r_0}} \quad (A.17)$$

$$T_{0(t)} = -\frac{j}{\alpha_{nml}\mathbb{D}F\delta_r} \frac{1}{1-\frac{\delta_r}{2r_0}} e^{-\alpha_{nml}\mathbb{D}t} + T_0^* \quad (A.18)$$

$$T_{(t)} = -\frac{j}{\alpha_{nml}\mathbb{D}F\delta_r} \frac{1}{1-\frac{\delta_r}{2r_0}} + T_0^* e^{\alpha_{nml}\mathbb{D}t} \quad (A.19)$$

Inserting the initial conditions $\frac{\partial T_{(0)}}{\partial t} = \frac{j}{F\delta_r} \frac{1}{1-\frac{\delta_r}{2r_0}}$ and the expression for $\alpha_{nml}$, we finally get for the solution of the time dependency.

$$T_{nml(t)}^* = \frac{j}{\mathbb{D}F\delta_r} \frac{1}{1-\frac{\delta_r}{2r_0}} \frac{1}{\frac{\lambda_{nl}^2}{r_o^2} + \frac{m^2\pi^2}{L^2}} \left(1 - e^{-\left(\frac{\lambda_{nl}^2}{r_o^2} + \frac{m^2\pi^2}{L^2}\right)\mathbb{D}t}\right)$$
$$(A.20)$$

Merging all the partial solutions together and considering the hydrogen source term $Q$ and the indici for the solutions ($\to n, m$ and $l$), we get $c_f$ (equation 4). This equation is best implemented in computer programmes such as Matlab. The Gibbs ringing phenomena at the edges of $R$, $\Theta$ and $Z$ may not be pronounced because these are a maximum at $t = 0$ where the value of $c$ is $c_0$ and vanish with time, depending on the diffusion coefficient $\mathbb{D}$.

### Appendix A.3. Particulate Solution for Kinetic Saturation $c_s$

The exact same derivation of the particulate solution for the case of kinetic saturation ($Q = k\left(1 - \frac{c_s}{c_\infty}\right) \in \omega$) will be extremely difficult because one needs to consider the quotient of two sums when solving the derivatives. Furthermore, using the variation of the constant ($c_s = f_{(t)}c_h$) is also challenging because the derived term for $f_{(t)}$ depends on $c_h$ and is thus not exclusively a function of time any more. Due to this and to the best of our knowledge, an explicit analytical solution of this equation for the case of kinetic saturation lies beyond the scope of this study and will be investigated in future works.

To still be able to derive solutions from this equation and to reduce computational efforts, the particulate solution was approximated over a time series of multiple homogeneous solutions. Calculating the homogeneous solution $c_h$ for a short time interval $t \to t + \Delta t$ and then normalising to the source term $Q$ for the existing solution will gradually approximate to the case of kinetic saturation. For a given time $t$ and a small time interval $\Delta t$, we can thus write.

$$c_{s(t+\Delta t)} = c_{s(t)} + k\left(c_\infty - c_{s(t)}\right)\Delta t \qquad (A.21)$$

Given the dependency of equation A.21 with time, we can successively solve the entire time series, starting from the initial value $c_{s(t=0)}$. Please note the initial value for the particulate solution with kinetic saturation and the homogeneous solution are identical ($c_{s(t=0)} = c_{h(t=0)}$). This method, however, may require significant computational resources when calculating long time intervals (logarithmic time axes) and is even prone to errors when the time step becomes too large. We hence set an internal limit of the maximum time step $\Delta t$ such that the concentration in the defect domain $\omega$ must not exceed 10 % of the saturation value ($c_s \leqslant 1.10\, c_\infty$).